Author Manuscript

Author Manuscript

Author Manuscript

Author Manuscript

HHS Public Access

Author manuscript

Int J Artif Organs. Author manuscript; available in PMC 2016 October 17.

Published in final edited form as:

Int J Artif Organs. 2016 October 10; 39(8): 421–430. doi:10.5301/ijao.5000520.

Partial LVAD restores ventricular outputs and normalizes LV but not RV stress distributions in the acutely failing heart in silico

Kevin L. Sack[1], **Brian Baillargeon**[2], **Gabriel Acevedo-Bolton**[3], **Martin Genet**[3,4,5], **Nuno Rebelo**[2], **Ellen Kuhl**[6], **Liviu Klein**[7], **Georg M. Weiselthaler**[3], **Daniel Burkhoff**[8], **Thomas Franz**[1,9], and **Julius M. Guccione**[3]

[1]Division of Biomedical Engineering, Department of Human Biology, University of Cape Town, Cape Town - South Africa [2]Dassault Systèmes Simulia Corporation, Fremont, CA - USA [3]Department of Surgery, University of California at San Francisco, San Francisco - USA [4]Marie-Curie International Outgoing Fellow, Palaiseau - France [5]Institute for Biomedical Engineering, University and ETH Zürich, Zurich - Switzerland [6]Departments of Mechanical Engineering, Bioengineering and Cardiothoracic Surgery, Stanford University, Stanford, CA - USA [7]Department of Medicine, University of California at San Francisco, San Francisco - USA [8]Department of Medicine, Columbia University, New York, NY - USA [9]Bioengineering Science Research Group, Engineering Sciences, Faculty of Engineering and the Environment, University of Southampton, Southampton - UK

Abstract

Purpose—Heart failure is a worldwide epidemic that is unlikely to change as the population ages and life expectancy increases. We sought to detail significant recent improvements to the Dassault Systèmes Living Heart Model (LHM) and use the LHM to compute left ventricular (LV) and right ventricular (RV) myofiber stress distributions under the following 4 conditions: (1) normal cardiac function; (2) acute left heart failure (ALHF); (3) ALHF treated using an LV assist device (LVAD) flow rate of 2 L/min; and (4) ALHF treated using an LVAD flow rate of 4.5 L/min.

Methods and Results—Incorporating improved systolic myocardial material properties in the LHM resulted in its ability to simulate the Frank-Starling law of the heart. We decreased myocardial contractility in the LV myocardium so that LV ejection fraction decreased from 56% to 28%. This caused mean LV end diastolic (ED) stress to increase to 508% of normal, mean LV end systolic (ES) stress to increase to 113% of normal, mean RV ED stress to decrease to 94% of normal and RV ES to increase to 570% of normal. When ALHF in the model was treated with an LVAD flow rate of 4.5 L/min, most stress results normalized. Mean LV ED stress became 85% of

This article is published by Wichtig Publishing and licensed under Creative Commons Attribution-NonCommercial-NoDerivatives 4.0 International (CC BY-NC-ND 4.0). Any commercial use is not permitted and is subject to Publisher's permissions. Full information is available at www.wichtig.com

Corresponding author: Julius M. Guccione, Jr., PhD, Professor, Division of Adult Cardiothoracic Surgery, Department of Surgery, School of Medicine, UCSF, 1657 Scott St., Mount Zion Harold Brunn Institute for Cardiovascular Research, Room 219, San Francisco, 94143 CA, USA, julius.guccione@ucsfmedctr.org.

Disclosures

Conflicts of interest: Brian Baillargeon and Nuno Rebelo are employees of Dassault Systèmes Simulia Corporation, Fremont, CA, USA. Julius Guccione is a consultant for Dassault Systèmes Simulia Corporation, Fremont, CA, USA.

Author Manuscript Author Manuscript Author Manuscript Author Manuscript

normal, mean LV ES stress became 109% of normal and mean RV ED stress became 95% of normal. However, mean RV ES stress improved less dramatically (to 342% of normal values).

Conclusions—These simulations strongly suggest that an LVAD is effective in normalizing LV stresses but not RV stresses that become elevated as a result of ALHF.

Keywords

Finite element method; Mechanical circulatory support; Realistic simulation; Ventricular function; Ventricular assist device

Introduction

Heart failure (HF) is a highly significant medical and economic problem afflicting an estimated 5.7 million Americans (1). Projections show that the prevalence of HF will increase 46% from 2012 to 2030, resulting in >8 million adults with HF (2). In 2012, the total cost for HF was estimated to be $30.7 billion. Of this total, 68% was attributable to direct medical costs related to hospitalizations (2). Projections show that by 2020, the total cost of HF will increase almost 127% to $69.7 billion from 2012 (2).

Left ventricular assist devices (LVADs) are a novel strategy for HF treatment, whereby the heart is provided with sufficient mechanical circulatory support to allow for offloading, which in turn promotes myocardial remodeling and recovery (3-5). The first-generation pulsatile flow devices have been replaced by newer generation continuous-flow LVADs that are smaller and more durable (6). In particular, LVADs, which can be implanted minimally invasively without sternotomy or cardiopulmonary bypass, remove some of the large risks associated with major surgery (7). These devices can deliver a range of flow output between 2-10 L/min (8), depending on the level of support needed. These improvements in device technology, coupled with greater clinical expertise surrounding LVADs, led to a decrease in patient risk over the last decade, making LVAD treatment an increasingly viable option for many patients (9). Furthermore, roughly 5% of LVAD-treated patients experience a full recovery, allowing for reduced support and, in some cases, device explantation (10, 11). Recent results show that miniaturized, less invasive, partial-support devices operating at low flow rates may have the potential to be used in more patients, particularly those with INTERMACS classification 4 and greater (12, 13).

Although clinical expertise regarding LVADs is increasing, the exact mechanisms responsible for myocardial recovery and reversal of HF are still not fully understood, limiting the ability to predict long-term function, durable recovery or remission of HF (10, 14). Computational studies have already been identified as a means to accelerate successful LVAD design and treatment protocols due to the inherent ability of cheaply and efficiently perturbing treatment parameters (15). Additionally, realistic computational models provide a wealth of information for clinical decision making (16), and may elucidate mechanical cues responsible for recovery that are otherwise unobtainable.

In this novel computational study concerned with the normal human heart, acute left HF, and LVAD therapy, we sought to detail significant improvements in the systolic material

Author Manuscript Author Manuscript Author Manuscript Author Manuscript

properties of the Dassault Systèmes Living Heart Model (LHM) and use it to compute left and right ventricular myofiber stress distributions under the following 4 conditions: (1) normal cardiac function; (2) acute left HF with an LV ejection fraction (EF) of 28%; (3) acute left HF using an LVAD flow rate of 2 L/min; and (4) acute left HF treated using an LVAD flow rate of 4.5 L/min. Relatively few computational studies have investigated the effect of LVADs on cardiac function utilizing realistic geometries (17, 18) due to the complexities involved, and to the best of our knowledge, our study is the first to present stress and strain results in both ventricles.

Methods

Whole heart modeling of the normal human heart

Baillargeon et al (19) created a finite element model of the whole heart on the basis of the existing solid model illustrated in Figure 1A. This made it possible to model all 4 chambers as electrically excitable, deformable, hyperelastic, electroactive bodies connected via in-flow and out-flow conditions of viscous resistance type (19). We refer the interested reader to Baillargeon et al (19) for the full description of the model, including the continuum model of electro-mechanical coupling, the balance equations, and the constitutive equations. Here we only present the changes in the LHM that were pertinent to this study.

The passive material response of the cardiac tissue uses an anisotropic hyperelastic formulation based on that proposed by Holzapfel and Ogden (20). In the LHM, this response appears to be more stable than the Fung response (21). The deviatoric and volumetric responses are governed by the strain energy potentials in Equations [1 and 2], with parameters defined in Table I.

$$\Psi_{dev}=\frac{a}{2b}e^{b(l_1-3)}+\sum_{i=f,s}\frac{a_i}{2b_i}\left\{e^{b_i(l_{4i}-1)^2}-1\right\}+\frac{a_{fs}}{2b_{fs}}\left\{e^{b_{fs}\left(l_{8\quad fs}\right)^2}-1\right\} \quad \text{Eq. [1]}$$

$$\Psi_{vol}=\frac{1}{D}\left(\frac{J^2-1}{2}-ln\left(J\right)\right). \quad \text{Eq. [2]}$$

The passive model parameters used in our study follow from the revised parameters presented in Baillargeon et al (22), which improved the LHM's performance in line with physiological expectations. This material model, Equations [1 and 2], ensures that the material exhibits the well-documented exponential and anisotropic response to strain (23-25) while enforcing near incompressibility.

Improvements to the Living Heart Model

This study incorporates recent improvements to the active-tissue material model, intended to capture the Frank-Starling effect (i.e., the strength of the heart's systolic contraction is directly proportional to its diastolic expansion). The active tissue response now contains

Author Manuscript Author Manuscript Author Manuscript Author Manuscript

length-dependent considerations of regional sarcomere lengths when the active response is determined. This affects the stress components in the fiber and sheet directions in the constitutive model.

The active stress in the cardiac muscle fiber direction is now defined by the following time-varying elastance model (26):

$$\sigma_{af}\left(t, E_{ff}\right) = \frac{T_{max}}{2} \frac{Ca_0^2}{Ca_0^2 + ECa_{50}^2\left(E_{ff}\right)} \left(1 - cos\left(\omega\left(t, E_{ff}\right)\right)\right), \quad \text{Eq. [3]}$$

where

$$ECa_{50}\left(E_{ff}\right) = \frac{Ca_{0_{max}}}{\sqrt{e^{B\left(l\left(E_{ff}\right) - l_0\right)} - 1}} \quad \text{Eq. [4]}$$

$$\omega\left(t, E_{ff}\right) = \begin{cases} \pi \frac{t}{t_0}, & \text{when} \quad 0 \leq t \leq t_0 \\ \pi \frac{t - t_0 + t_r\left(l\left(E_{ff}\right)\right)}{t_r} & \text{when} \quad t_0 \leq t \leq t_0 + t_r\left(l\left(E_{ff}\right)\right) \\ 0, & \text{when} \quad t \geq t_0 + t_r\left(l\left(E_{ff}\right)\right) \end{cases} \quad \text{Eq. [5]}$$

$$t_r\left(l\right) = ml + b, \quad \text{Eq. [6]}$$

$$l\left(E_{ff}\right) = l_r\sqrt{2E_{ff} + 1}, \quad \text{Eq. [7]}$$

with parameters as defined in Table I. The mathematical description of active tension, Equations [3-7], ensures a smooth yet steep transition from zero to peak active tension at time t_0 and then a smooth decline back to zero for the specified relaxation time t_r.

As in previous work (19), the total stress in the fiber direction, σ_f, is equal to the active stress, σ_{af}, plus the passive stress, σ_{pf}:

$$\sigma_f = \sigma_{pf} + \sigma_{af} \quad \text{Eq. [8]}$$

Total stress in the sheet direction, σ_s, is the sum of the passive stress, σ_{ps}, and a fraction of the stress in the fiber direction, $n\sigma_{af}$ (where n is a scalar value less than 1.0 and represents the interaction between the adjacent muscle fibers):

Author Manuscript Author Manuscript Author Manuscript Author Manuscript

$$\sigma_s = \sigma_{ps} + n\sigma_{af} \quad \text{Eq. [9]}$$

The value of n affects not only the total contractility of the chambers, but also the degree of twist developed in the chamber during the cardiac cycle. The magnitude of contractility for each chamber was tuned to provide the appropriate EF for that chamber. This involved tuning T_{max}, n (to limit the twist of the LV and RV) and l_0.

Figure 1B shows the mechanical finite-element model of Zygote's second-generation solid heart geometry, which is discretized with more than 480,000 mixed elements, resulting in 130,290 nodes and 443,564 mechanical degrees of freedom. Figure 1C illustrates the electrical finite-element model, high-lighting the representative Purkinje fiber network, discretized by over 600 1D linear conduction elements embedded in the same mesh for the ventricles and atria as the mechanical model. The muscle fiber model, shown in Figure 1D, is prescribed to all solid elements in the model.

Living Heart Model with simulated acute left heart failure

Systolic heart failure due to left ventricular dysfunction refers to the severely impaired heart function that results from reduced LV contractility. Loss of systolic function causes reduced ventricular emptying, resulting in increased LV end-diastolic (ED) volume and pressure. This acute left heart failure (ALHF) is the pathological condition simulated in this study. The loss of contractility was simulated by the single adjustment of parameter T_{max} in the LV until an EF symptomatic of HF was produced in the LHM. This simulation resulted in an EF of 28% with a value of T_{max} at 25% of its normal value. Healthy values for EF are set at values >50%, with 35-50% representing a "grey area" for clinical diagnosis and values <35% clearly indicative of HF (27, 28). Average EF measurements of patients enrolled in larger trials report even lower values ranging from 27% to 34% (29, 30), placing our simulated ALHF model as a prominent dysfunction well away from "grey area" values.

In silico simulation of LVAD in the acutely failing human heart

By considering the newer-generation continuous flow devices, whereby the small size of the LVAD allows for minimally invasive attachment, only the effect of the device is simulated, i.e., the flow conditions between the cavities are modified to simulate differing LVAD support. The LVAD inflow cannula tip is inserted into the LV, and the outflow, connecting the device to the arterial network, is usually attached via the aorta. The acutely failing human heart model described above was further modified to simulate the effect of the LVAD through the introduction of an additional fluid exchange between the beating LV fluid cavity and the arterial system. The circulatory system included lumped compliance and resistance parameters representing the viscous fluid exchanges amongst the 4-chamber heart, the arterial system, the pulmonary system, and the major linking vasculature. A schematic diagram outlining the fluid connections between the electro-mechanically driven heart and the lumped circulatory system with the LVAD is presented in Figure 2. The LVAD has an additive contribution to the arterial system that provides a constant blood flow that complements the LV ejection output while reducing LV physical diastolic loading. In these

Author Manuscript Author Manuscript Author Manuscript Author Manuscript

simulations, output from the LVAD was set at 2.0 L/min and again at 4.5 L/min, indicative of the range of realistic output from the miniaturized newer-generation LVADs (8, 12). Aside from the LVAD, all other fluid exchanges are pressure-driven by the realistic mechanical model of the 4-chamber heart.

Because the LVAD resides outside the heart and is surgically connected to the LV via a small inflow cannula, the restraint on LV motion is considered negligible and is ignored in the model set up. To restrict rigid body motion, Dirichlet boundary conditions are applied to the truncated branches stemming off of the aortic arch (see Fig. 2). The geometric representations of the aorta, pulmonary trunk, and vena cavae are bypassed by the lumped blood-flow model and are connected passively to the model purely as a means to enforce realistic boundary conditions.

Results

The LHM simulated heart function within the range for healthy human adults; functional parameters are presented in Table II.

The effects of reduced contractility in the LV cause dramatic changes throughout the cardiovascular system. The LV experiencing ALHF undergoes volumetric overloading throughout the cycle, which results in a significant elevation in diastolic pressures. Specifically, there were increases in the ED volume of 35% and the ED pressure of 159%. This increased cavity volume of the acutely failing LV throughout the cardiac cycle results in a sustained state of elongation for the cardiac tissue throughout the cycle. In addition, the dependence of RV mechanics on healthy LV function is made clear by the degree of impairment the RV experiences. Both diastolic and systolic RV function is significantly compromised by the enlarged LV.

The introduction of the LVAD changes the hemodynamic state of the entire cardiovascular system. The additional flow conditions simultaneously reduce the diastolic loading of the LV and increase the arterial pressure, establishing a new equilibrium that generates more positive cardiac outcomes throughout the heart. As the flow rate of the device increases, the reduced loading shifts the ED state of the failing LV towards normal values. As LVAD flow increases, the LV PV-loop becomes more triangular, indicative of the device's effect during the normally isovolumetric periods of the cardiac cycle (31, 32).

Stroke volume (SV) and EF quantified from the ED and endsystolic (ES) volumes alone significantly misrepresent the total LV output by neglecting the volume contribution of the device over the other stages of the cardiac cycle. Presented in Table II alongside SV are the total output results for the LV over a single cardiac cycle and the effective EF, which include contributions from the LVAD. Whereas the EF of the LV in the untreated acutely failing heart is 28%, the effective EF of the LV rises to 34% and then 55% for partial LVAD assistance operating at 2.0 L/min to 4.5 L/min, respectively. This was accompanied by a reduction of the LV ED volume through LVAD operation to within 1.5% of the normal LV ED volume. Additionally, the LVAD significantly reduced ED pressure by 10.1-20.8 mmHg operating at this range (2.0-4.5 L/min). LVAD operation shifts pressures in the LV towards

Author Manuscript Author Manuscript Author Manuscript Author Manuscript

normal ranges over the cardiac cycle, as seen in Table II. The change of function of the RV is significantly dependent on the LV. Because the model circulatory system is a closed loop with pressures, volumes, and resulting flows that depend on the entire system, the RV pump function will naturally adjust to match the pump function of the LV. This is seen in Table II, which shows the SV of the RV matches closely with the total output of the LV in all simulated cases. Although cavity pressure and volume in the RV are not as significantly affected as in the LV, the overall function of the RV is still just as severely compromised due to its dependence on LV function. This dependence works both ways, as seen in the case of LVAD operation at 4.5 L/min, which brings the effective SV and EF for both ventricles within 2% of normal values.

Strain results

Strain profiles of the heart (along the myofiber direction) at ED are presented in Figure 3. The elevated strains experienced in the heart with ALHF, which lead to adverse remodeling, are clearly decreased by the use of the partial LVAD throughout the cardiac cycle. The models with incorporated partial LVADs predict a minor reduction of strains for LVAD operation of 2 L/min and a significant reduction in strains for LVAD operation at 4.5 L/min. Strains are critically reduced at ED (Fig. 3), the point in the cardiac cycle which would subject the LV to largest strains.

Stress results

Stress distributions for myofiber stress (along the local muscle fiber direction) are presented in Figure 4 at ED and Figure 5 at ES. The volumetric-averaged myofiber stress was calculated at ED and ES and the mean values with standard deviations are presented in Table III for the RV and LV separately. The resulting mean myofiber stress found in the healthy LV was 1.47 ± 20.72 kPa at ED, and 14.45 ± 106.72 kPa at ES. Impaired LV contractility resulted in an increase of LV mean myofiber stress to 7.47 kPa, roughly 5 times the normal values at ED. Increases were similar in RV myofiber stress at ES. For partial LVAD assistance, myofiber stress was significantly reduced in the LV, returning to lower values of 4.00 and 1.26 kPa for LVAD operation at 2.0 and 4.5 L/min, respectively. This is seen qualitatively in Figure 4, which also shows the assisted LV presenting a more ellipsoidal shape at ED compared to the heart with ALHF. Myofiber stress distributions throughout the cardiac cycle for all 4 cases are shown in the online-only supplementary video 1 (available online as supplementary material at www.artificial-organs.com).

Discussion

The improved LHM allowed us to model the effects of varying flow rate on an LVAD connected to a diseased heart experiencing ALHF. Using the LHM, and simulating a continuous-flow LVAD between 2.0 and 4.5 L/min, provided a brief in silico investigation on the effect partial LVAD may have on the acutely failing human heart. Monitoring left and right ventricular mechanics, our study presented clear improvements to cardiac function in the acutely failing human heart. This was seen in the return to normal values for SVs and EFs in both ventricles with LVAD operation at 4.5 L/min. The most dramatic improvement, however, was seen in the reduction of pressure, chamber size and stress in the LV at ED. The

Author Manuscript Author Manuscript Author Manuscript Author Manuscript

reduction in chamber size and LV preload due to LVADs is well established in clinical findings (33, 34) and other numerical investigations (18, 32, 35).

Mean stress results found in our study for the LV at ED and ES match closely to the mean reported values in a recent study outlining stress values for healthy human LV cardiac models (21). The distribution of stresses is much larger in our model because of its more complex geometric representation and the use of a more sophisticated material model that includes regionally timed activation due to the electro-mechanical coupling (19). Presented alongside Figures 4 and 5 (or the online-only supplementary video clip), these values are given greater context: the beating heart is not a homogenous entity and experiences a complex combination of compressive and tensile stresses throughout the cardiac cycle.

The reduction of wall stress found at ED due to LVAD use is critically important. Changes in mechanical loading conditions, particularly ventricular wall stress, are thought to be a fundamental trigger for remodeling in the heart (36-38). Forces or stresses in the intact heart wall cannot be measured directly (39), and although imaging techniques can provide accurate strain information from in vivo hearts, this does not translate to stress without severe assumptions. For example, Laplace's law, used to estimate average stress across the heart wall, makes considerable assumptions with respect to the cardiac structure and provides considerably different results compared to anatomically accurate finite element models (40).

The modest changes to ES stress in the LV due to ALHF and subsequent LVAD operation are intriguing. A recent finite element study of an isolated LV with reduced contractility and LVAD support also reported modest changes in ES stress due to LVAD support (35). It is possible that decreased loading of the acutely failing LV at ED, which would result in a relatively reduced contraction, is offset by the increase in arterial pressure that the LV is working against during ejection, resulting in small changes to ES stress. A similar argument could be made for the changes from the normal to acutely failing heart.

A physiological improvement in contractility for patients with LVADs is likely due to recovery post-unloading, as our model shows that the reduction in ED preload does not directly improve contractility. This can be clearly seen in Figure 4, whereby only the healthy heart shows that significant portions of the LV, beyond papillary muscle, experience compressive stress. Although LVAD support reduces the LV chamber volume at ED, chamber volume remains inflated for the remainder of the cardiac cycle. Our model shows that LVAD operation mitigates some of the elevated stresses experienced in the RV at ES, but the overall mean stress in the RV remains high (Tab. III). The elevated stresses sustained throughout LVAD support in the RV at ES are likely due to the mechanical and structural dependence of the RV on LV contractility, which remain impaired despite LVAD operation. Since the active contraction law in our model includes length-dependent activation, the resulting contractile force within the LV decreases with LVAD operation – as strain reduction is a primary outcome of LVAD operation. This is seen in Figure 5, where the unassisted heart with ALHF displays increased wall thickness at ES compared to the assisted hearts with ALHF. It is likely that the functional improvements made to the RV through the introduction of the LVAD are partially offset by negative secondary outcomes on the RV.

Author Manuscript Author Manuscript Author Manuscript Author Manuscript

This is in line with clinical findings, which report positive (41), neutral (42) and negative outcomes (43, 44) on RV function through LVAD use. However, reports of RV failure occurring in 10%-30% of patients treated with LVADs (43-47) – depending on the severity of RV failure, the characteristics of the study population, and the type of LVAD – suggests that the balance between positive and negative outcomes on the RV is often missed. Although our simulated results showed that stresses in the LV were normalized through LVAD use, RV stresses were not as easily recovered. The quantification and monitoring of RV stress may play a critical role in optimizing LVAD treatment to avoid RV dysfunction.

This is the fourth study utilizing the LHM and the first to include length-dependent activation in simulating the contractile behavior of the heart in systole. To the best of our knowledge, this is also the first computational LVAD study that utilizes a 4-chamber anatomical description of the heart. This allowed us to capture the mechanical changes in the ventricles due to reduced LV contractility with and without assistance. The return to normal values for SVs and EFs in both ventricles supports the position that partial LVADs may provide significant benefit for patients with ALHF (12, 32). This position was further supported by a strain and stress analysis, showing the reduction of stress in the LV and a qualitative return to shape through the influence of partial LVADs.

The ability to accurately account for and predict changes to the myofiber stress in the heart could significantly aid clinical decision making and therapy optimization for patients undergoing LVAD treatment, whereby stress-driven adverse remodeling could be mitigated or even reversed (48). Realistic, physics-based computational modeling offers a potential means to tailor treatments in a patient-specific framework. The modeling presented in this study could be advanced by including patient-specific data and utilized in clinical decision-making for patients who may benefit from partial, instead of full, LV support.

Although the LHM exemplifies state-of-the-art modeling techniques in cardiovascular computational modeling, limitations still apply (22). The functional improvements seen in the LHM model with ALHF treated with a partial LVAD are in part facilitated by the idealized in silico description of cardiac tissue, modeled here as purely elastic, and as such, the changes in deformation between healthy and ALHF are inherently more recoverable than such changes would be in a chronically remodeled failing heart. Here, the heart topology was unaltered from the normal heart and ALHF was induced by lowering the contractility in the LV only. In this sense, adverse remodeling due to chronic LHF and reverse remodeling due to the partial LVAD were neglected. The model can be improved by enriching the kinematic and constitutive models to include growth modeling to account for chronic remodeling and reverse remodeling phenomena (49). Future improvements to coupled fluid-structure interactions and patient-specific features would provide a broader and increasingly reliable set of model predictions. Furthermore, our simulated LVAD flow was created using unchanging constant flow specifications, whereas real-life LVADs perform according to motor function and pressure gradients. As such, our simulated LVAD flow is insensitive to mean arterial pressure (afterload), which would induce fluctuations in flow-rate performance. A description of LVAD flow rate sensitive to afterload would also provide another level of sophistication to the model.

Author Manuscript Author Manuscript Author Manuscript Author Manuscript

In conclusion, our study advanced the systolic material description of the Dassault Systèmes LHM to include length-dependent activation. We used this improved LHM to simulate ALHF through the overall reduction in contractility of the LV and simulated the use of a partial-support LVAD on that heart. Our simulations strongly suggest that an LVAD is effective in normalizing LV stresses but not RV stresses that become elevated as a result of ALHF.

Supplementary Material

Refer to Web version on PubMed Central for supplementary material.

Acknowledgments

This work was performed as part of the Living Heart Project. The authors thank Pamela Derish in the Department of Surgery, UCSF, for proofreading the manuscript.

Financial support: This work was supported by NIH grants R01-HL-077921 and R01-HL-118627 (J.M. Guccione) and U01-HL-119578 (J.M. Guccione and E. Kuhl); K25-NS058573-05 (G. Acevedo-Bolton); and Marie-Curie International Outgoing Fellowship within the 7th European Community Framework Program (M. Genet). Ellen Kuhl also acknowledges support by the National Science Foundation CAREER award CMMI 0952021, by the National Science Foundation INSPIRE grant 1233054, and by the National Institutes of Health grant U54 GM072970. K.L. Sack acknowledges financial support through a scholarship from the Oppenheimer Memorial Trust. K.L. Sack and T. Franz acknowledge financial support from the National Research Foundation of South Africa.

References

1. Go AS, Mozaffarian D, Roger VL, et al. Heart disease and stroke statistics - 2014 update: a report from the American Heart Association. Circulation. 2014; 129(3):e28–e292. [PubMed: 24352519]
2. Heidenreich PA, Albert NM, Allen LA, et al. Forecasting the impact of heart failure in the United States: a policy statement from the American Heart Association. Circ Heart Fail. 2013; 6(3):606–619. [PubMed: 23616602]
3. Birks EJ, Tansley PD, Hardy J, et al. Left ventricular assist device and drug therapy for the reversal of heart failure. N Engl J Med. 2006; 355(18):1873–1884. [PubMed: 17079761]
4. Burkhoff D, Klotz S, Mancini DM. LVAD-induced reverse remodeling: basic and clinical implications for myocardial recovery. J Card Fail. 2006; 12(3):227–239. [PubMed: 16624689]
5. Wohlschlaeger J, Schmitz KJ, Schmid C, et al. Reverse remodeling following insertion of left ventricular assist devices (LVAD): a review of the morphological and molecular changes. Cardiovasc Res. 2005; 68(3):376–386. [PubMed: 16024006]
6. McIlvennan CK, Magid KH, Ambardekar AV, Thompson JS, Matlock DD, Allen LA. Clinical outcomes after continuous-flow left ventricular assist device: a systematic review. Circ Heart Fail. 2014; 7(6):1003–1013. [PubMed: 25294625]
7. Meyns BP, Simon A, Klotz S, et al. Clinical benefits of partial circulatory support in New York Heart Association Class IIIB and Early Class IV patients. Eur J Cardiothorac Surg. 2011; 39(5): 693–698. [PubMed: 20934882]
8. Timms D. A review of clinical ventricular assist devices. Med Eng Phys. 2011; 33(9):1041–1047. [PubMed: 21665512]
9. Lampropulos JF, Kim N, Wang Y, et al. Trends in left ventricular assist device use and outcomes among Medicare beneficiaries, 2004-2011. Open heart. 2014; 1(1):e000109. [PubMed: 25332817]
10. Pan S, Aksut B, Wever-Pinzon OE, et al. Incidence and predictors of myocardial recovery on long-term left ventricular assist device support: Results from the United Network for Organ Sharing database. J Heart Lung Transplant. 2015; 34(12):1624–1629. [PubMed: 26442678]

Author Manuscript Author Manuscript Author Manuscript Author Manuscript

11. Mancini DM, Beniaminovitz A, Levin H, et al. Low incidence of myocardial recovery after left ventricular assist device implantation in patients with chronic heart failure. Circulation. 1998; 98(22):2383–2389. [PubMed: 9832482]
12. Sabashnikov A, Popov AF, Bowles CT, et al. Outcomes after implantation of partial-support left ventricular assist devices in inotropic-dependent patients: Do we still need full-support assist devices? J Thorac Cardiovasc Surg. 2014; 148(3):1115–1121. [PubMed: 25129605]
13. Mohite PN, Sabashnikov A, Simon AR, et al. Does CircuLite Synergy assist device as partial ventricular support have a place in modern management of advanced heart failure? Expert Rev Med Devices. 2014; 12(1):49–60. [PubMed: 25454250]
14. Helman DN, Maybaum SW, Morales DL, et al. Recurrent remodeling after ventricular assistance: is long-term myocardial recovery attainable? Ann Thoracic Surg. 2000; 70(4):1255–1258.
15. Marsden AL, Bazilevs Y, Long CC, Behr M. Recent advances in computational methodology for simulation of mechanical circulatory assist devices. Wiley Interdiscip Rev Syst Bio Med. 2014; 6(2):169–188. [PubMed: 24449607]
16. Sack KL, Davies NH, Guccione JM, Franz T. Personalised computational cardiology: Patient-specific modelling in cardiac mechanics and biomaterial injection therapies for myocardial infarction. Heart Fail Rev. Feb 1.2016 ePub ahead of print.
17. McCormick M, Nordsletten DA, Kay D, Smith NP. Simulating left ventricular fluid-solid mechanics through the cardiac cycle under LVAD support. J Comput Phys. 2013; 244:80–96.
18. Lim KM, Constantino J, Gurev V, Zhu R, Shim EB, Trayanova NA. Comparison of the effects of continuous and pulsatile left ventricular-assist devices on ventricular unloading using a cardiac electromechanics model. J Physiol Sci. 2012; 62(1):11–19. [PubMed: 22076841]
19. Baillargeon B, Rebelo N, Fox DD, Taylor RL, Kuhl E. The Living Heart Project: A robust and integrative simulator for human heart function. Eur J Mech A Solids. 2014; 48:38–47. [PubMed: 25267880]
20. Holzapfel GA, Ogden RW. Constitutive modelling of passive myocardium: a structurally based framework for material characterization. Philos Trans A Math Phys Eng Sci. 2009; 367(1902): 3445–3475. [PubMed: 19657007]
21. Genet M, Lee LC, Nguyen R, et al. Distribution of normal human left ventricular myofiber stress at end diastole and end systole: a target for in silico design of heart failure treatments. J Appl Physiol (1985). 2014; 117(2):142–152. [PubMed: 24876359]
22. Baillargeon B, Costa I, Leach JR, et al. Human Cardiac Function Simulator for the Optimal Design of a Novel Annuloplasty Ring with a Sub-valvular Element for Correction of Ischemic Mitral Regurgitation. Cardiovasc Eng Technol. 2015; 6(2):105–116. [PubMed: 25984248]
23. Demer LL, Yin FC. Passive biaxial mechanical properties of isolated canine myocardium. J Physiol. 1983; 339:615–630. [PubMed: 6887039]
24. Hunter PJ, McCulloch AD, ter Keurs HE. Modelling the mechanical properties of cardiac muscle. Prog Biophys Mol Biol. 1998; 69(2-3):289–331. [PubMed: 9785944]
25. Dokos S, Smaill BH, Young AA, LeGrice IJ. Shear properties of passive ventricular myocardium. Am J Physiol Heart Circ Physiol. 2002; 283(6):H2650–H2559. [PubMed: 12427603]
26. Walker JC, Ratcliffe MB, Zhang P, et al. MRI-based finite-element analysis of left ventricular aneurysm. Am J Physiol Heart Circ Physiol. 2005; 289(2):H692–H700. [PubMed: 15778283]
27. McMurray JJ, Adamopoulos S, Anker SD, et al. ESC Guidelines for the diagnosis and treatment of acute and chronic heart failure 2012. Eur J Heart Fail. 2012; 14(8):803–869. [PubMed: 22828712]
28. Mann, DL.; Zipes, DP.; Libby, P.; Bonow, RO. Braunwald's heart disease: a textbook of cardiovascular medicine. Elsevier Health Sciences; Philadelphia, PA: 2014.
29. Adams KF, Fonarow GC, Emerman CL, et al. Characteristics and outcomes of patients hospitalized for heart failure in the United States: rationale, design, and preliminary observations from the first 100,000 cases in the Acute Decompensated Heart Failure National Registry (ADHERE). Am Heart J. 2005; 149(2):209–216. [PubMed: 15846257]
30. Publication Committee for the VI. Intravenous nesiritide vs nitroglycerin for treatment of decompensated congestive heart failure: A randomized controlled trial. JAMA. 2002; 287(12): 1531–1540. [PubMed: 11911755]

Author Manuscript Author Manuscript Author Manuscript Author Manuscript

31. Wang Y, Loghmanpour N, Vandenberghe S, et al. Simulation of dilated heart failure with continuous flow circulatory support. PLoS One. 2014; 9(1):e85234. [PubMed: 24465511]
32. Morley D, Litwak K, Ferber P, et al. Hemodynamic effects of partial ventricular support in chronic heart failure: results of simulation validated with in vivo data. J Thorac Cardiovasc Surg. 2007; 133(1):21–28. [PubMed: 17198776]
33. Barbone A, Holmes JW, Heerdt PM, et al. Comparison of Right and Left Ventricular Responses to Left Ventricular Assist Device Support in Patients With Severe Heart Failure A Primary Role of Mechanical Unloading Underlying Reverse Remodeling. Circulation. 2001; 104(6):670–675. [PubMed: 11489773]
34. Levin HR, Oz MC, Chen JM, Packer M, Rose EA, Burkhoff D. Reversal of chronic ventricular dilation in patients with end-stage cardiomyopathy by prolonged mechanical unloading. Circulation. 1995; 91(11):2717–2120. [PubMed: 7758175]
35. Jhun CS, Sun K, Cysyk JP. Continuous flow left ventricular pump support and its effect on regional left ventricular wall stress: finite element analysis study. Med Biol Eng Comput. 2014; 52(12): 1031–1040. [PubMed: 25284220]
36. Matiwala S, Margulies KB. Mechanical approaches to alter remodeling. Curr Heart Fail Rep. 2004; 1(1):14–18. [PubMed: 16036020]
37. Sutton MGSJ, Sharpe N. Left ventricular remodeling after myocardial infarction pathophysiology and therapy. Circulation. 2000; 101(25):2981–2988. [PubMed: 10869273]
38. Pfeffer MA, Braunwald E. Ventricular remodeling after myocardial infarction. Experimental observations and clinical implications. Circulation. 1990; 81(4):1161–1172. [PubMed: 2138525]
39. Dorri F, Niederer PF, Lunkenheimer PP. A finite element model of the human left ventricular systole. Comput Methods Biomech Biomed Engin. 2006; 9(5):319–341. [PubMed: 17132618]
40. Zhang Z, Tendulkar A, Sun K, et al. Comparison of the Young-Laplace law and finite element based calculation of ventricular wall stress: implications for postinfarct and surgical ventricular remodeling. Ann Thorac Surg. 2011; 91(1):150–156. [PubMed: 21172505]
41. Küçüker SA, Stetson SJ, Becker KA, et al. Evidence of improved right ventricular structure after LVAD support in patients with end-stage cardiomyopathy. J Heart Lung Transplant. 2004; 23(1): 28–35. [PubMed: 14734124]
42. Maeder MT, Leet A, Ross A, Esmore D, Kaye DM. Changes in right ventricular function during continuous-low left ventricular assist device support. J Heart Lung Transplant. 2009; 28(4):360–366. [PubMed: 19332263]
43. Kavarana MN, Pessin-Minsley MS, Urtecho J, et al. Right ventricular dysfunction and organ failure in left ventricular assist device recipients: a continuing problem. Ann Thorac Surg. 2002; 73(3):745–750. [PubMed: 11899176]
44. Dang NC, Topkara VK, Mercando M, et al. Right heart failure after left ventricular assist device implantation in patients with chronic congestive heart failure. J Heart Lung Transplant. 2006; 25(1):1–6. [PubMed: 16399523]
45. Argiriou M, Kolokotron S-M, Sakellaridis T, et al. Right heart failure post left ventricular assist device implantation. J Thoracic Dis. 2014; 6(Suppl 1):S52–S59.
46. Baumwol J, Macdonald PS, Keogh AM, et al. Right heart failure and “failure to thrive” after left ventricular assist device: clinical predictors and outcomes. J Heart Lung Transplant. 2011; 30(8): 888–895. [PubMed: 21530314]
47. Kormos RL, Teuteberg JJ, Pagani FD, et al. Right ventricular failure in patients with the HeartMate II continuous-flow left ventricular assist device: incidence, risk factors, and effect on outcomes. J Thorac Ccardiovasc Surg. 2010; 139(5):1316–1324.
48. Drakos SG, Kfoury AG, Selzman CH, et al. Left ventricular assist device unloading effects on myocardial structure and function: Current status of the field and call for action. Curr Opin Cardiol. 2011; 26(3):245–255. [PubMed: 21451407]
49. Genet M, Lee LC, Baillargeon B, Guccione JM, Kuhl E. Modeling Pathologies of Diastolic and Systolic Heart Failure. Ann Biomed Eng. 2016; 44(1):112–127. [PubMed: 26043672]

Author Manuscript Author Manuscript Author Manuscript Author Manuscript

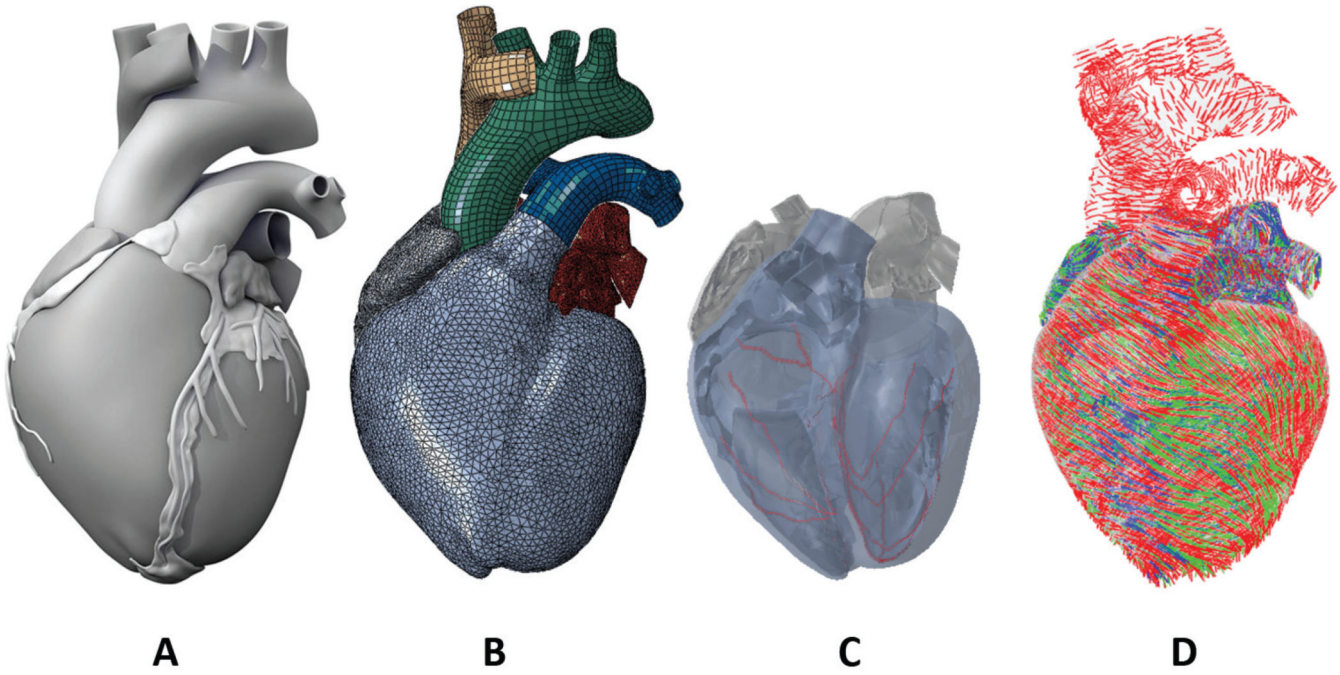

Fig. 1.

(**A**) Solid model of the human heart used as the basis for our improved model. It was created from computed tomography and magnetic resonance imaging; adapted with permission from (Zygote Media Group and Inc., 2014). (**B**) Mechanical finite element model of the human heart discretized with 449,560 linear tetrahedral elements, 12,915 linear quadrilateral shells, 7577 linear triangular shells, 636 linear truss elements, 16,824 rigid triangular elements, 130,290 nodes, and 443,564 mechanical degrees of freedom. (**C**) Electrical finite element model of the human heart discretized with 449,560 linear tetrahedral elements, 655 1D linear conduction elements (red), 103,770 nodes, and 103,770 electrical degrees of freedom. (**D**) Fiber orientations of the Living Heart Model.

Author Manuscript Author Manuscript Author Manuscript Author Manuscript

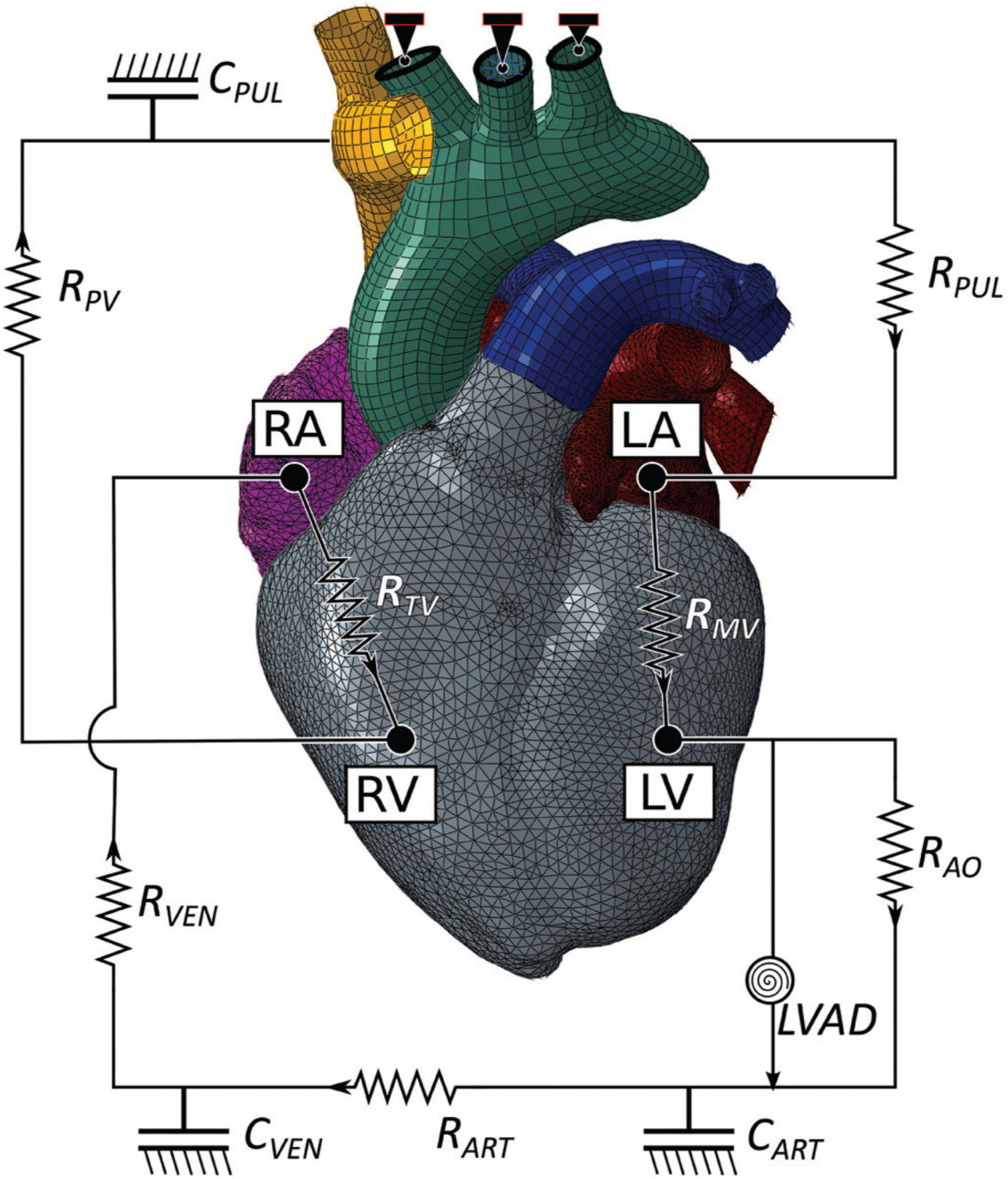

Fig. 2.

Schematic of the electromechanical model coupled with the circulatory system and LVAD. The truncated branched arteries from the aortic arch are fixed to prevent rigid body motion. R_{MV} is mitral valve resistance, R_{AO} is aortic valve resistance, C_{ART} is systemic arterial compliance, R_{ART} is systemic arterial resistance, C_{VEN} is venous compliance, R_{VEN} is venous resistance, R_{PV} is pulmonary valve resistance, C_{PUL} is pulmonary system compliance, R_{PUL} is pulmonary system resistance, and R_{TV} is tricuspid valve resistance.

Author Manuscript Author Manuscript Author Manuscript Author Manuscript

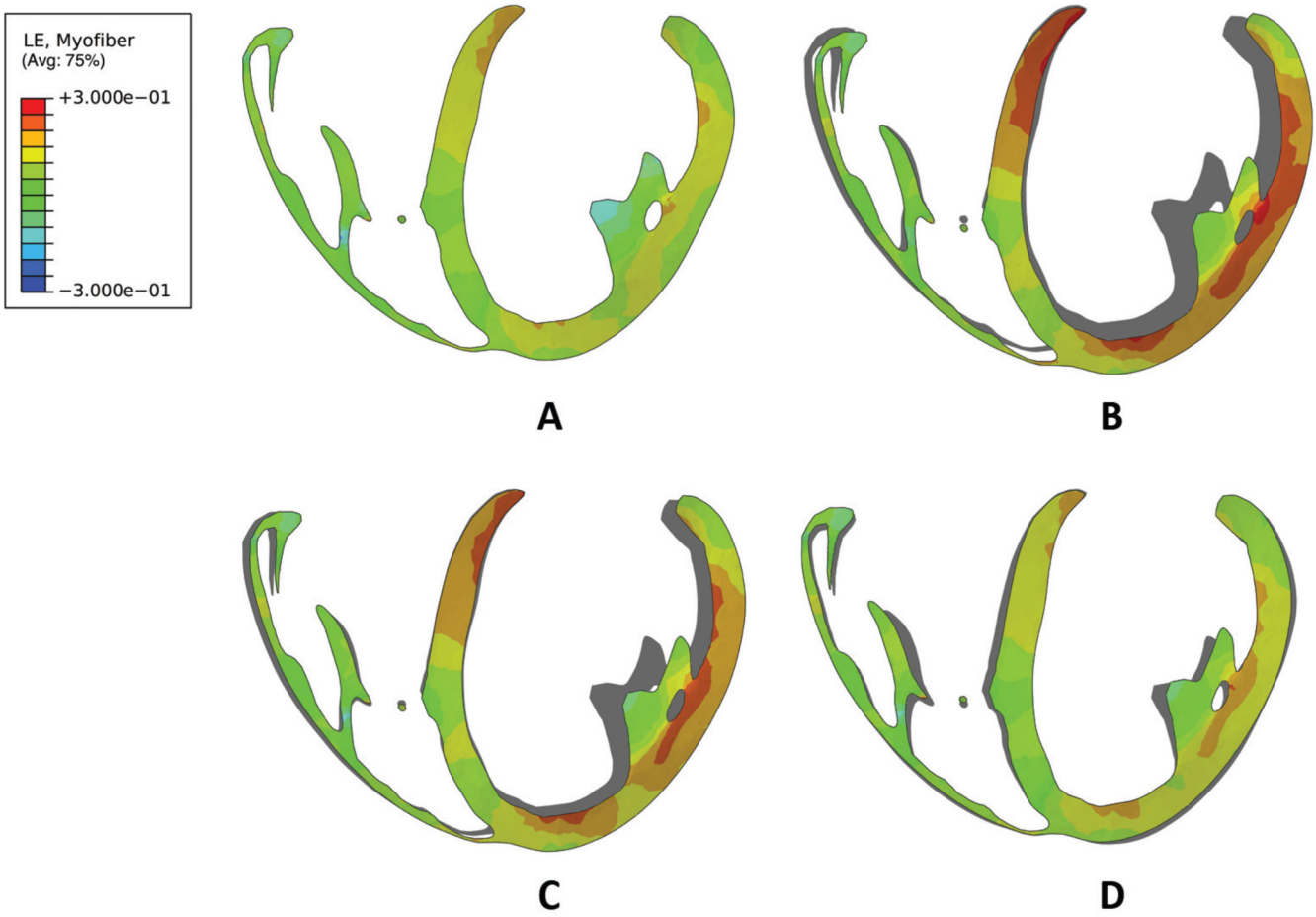

Fig. 3.

Long-axis profiles of the heart at the end of diastole showing contours of logarithmic myofiber strain for a normal healthy heart (**A**), a heart experiencing ALHF (**B**), a heart with ALHF and partial LVAD running at 2 L/min (**C**), and a heart with ALHF and partial LVAD running at 4.5 L/min (**D**). The deformed profile of the normal healthy heart (**A**) is placed behind profiles of cases (**B**) to (**D**) as a grey silhouette for comparison.

Author Manuscript Author Manuscript Author Manuscript Author Manuscript

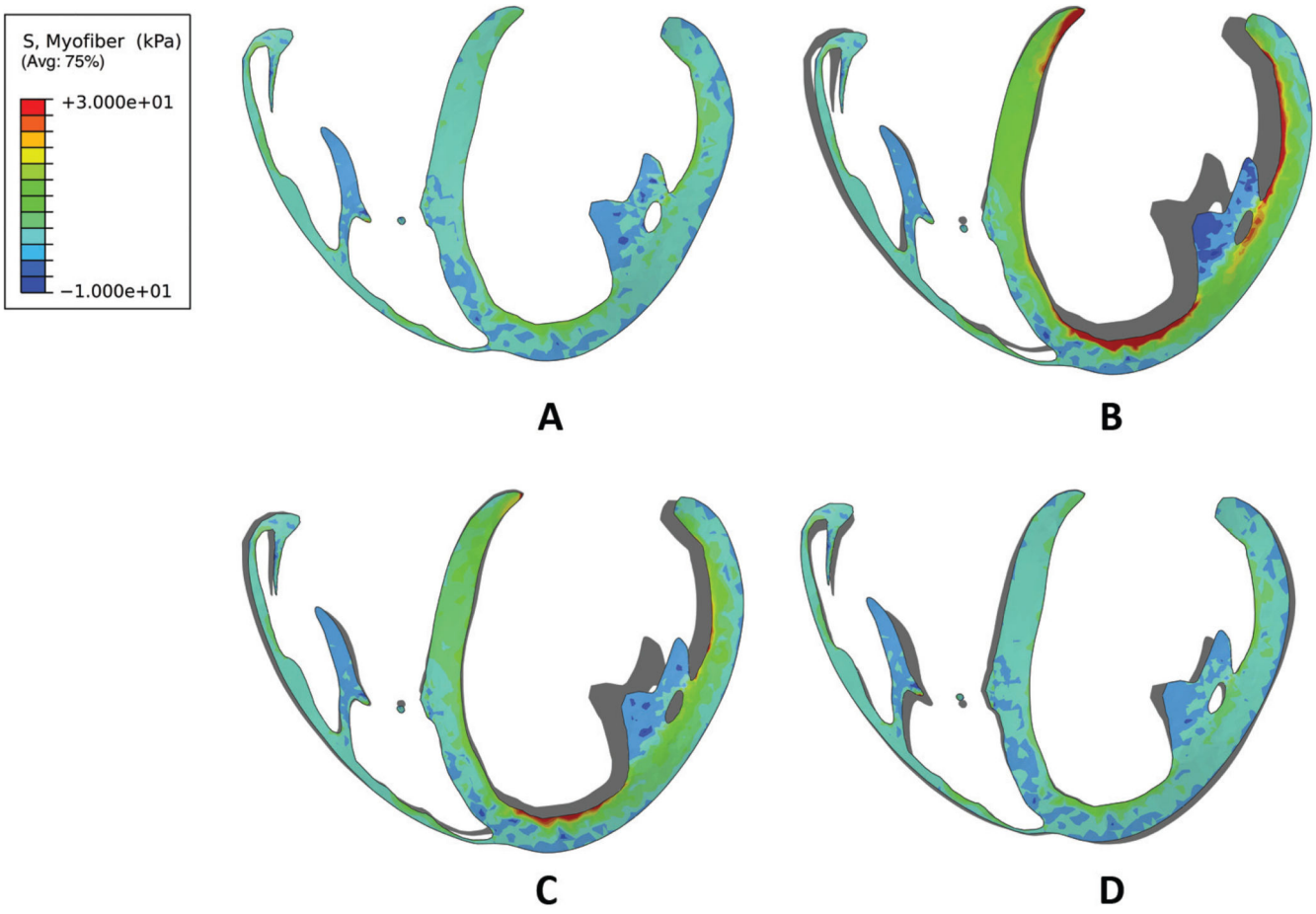

Fig. 4.

Long-axis profiles of the heart at the end of diastole showing contours of myofiber stress for a normal healthy heart (**A**), a heart experiencing ALHF (**B**), a heart with ALHF and partial LVAD running at 2 L/min (**C**), and a heart with ALHF and partial LVAD running at 4.5 L/min (**D**). The deformed profile of the normal healthy heart (**A**) is placed behind profiles of cases (**B**) to (**D**) as a grey silhouette for comparison.

Author Manuscript Author Manuscript Author Manuscript Author Manuscript

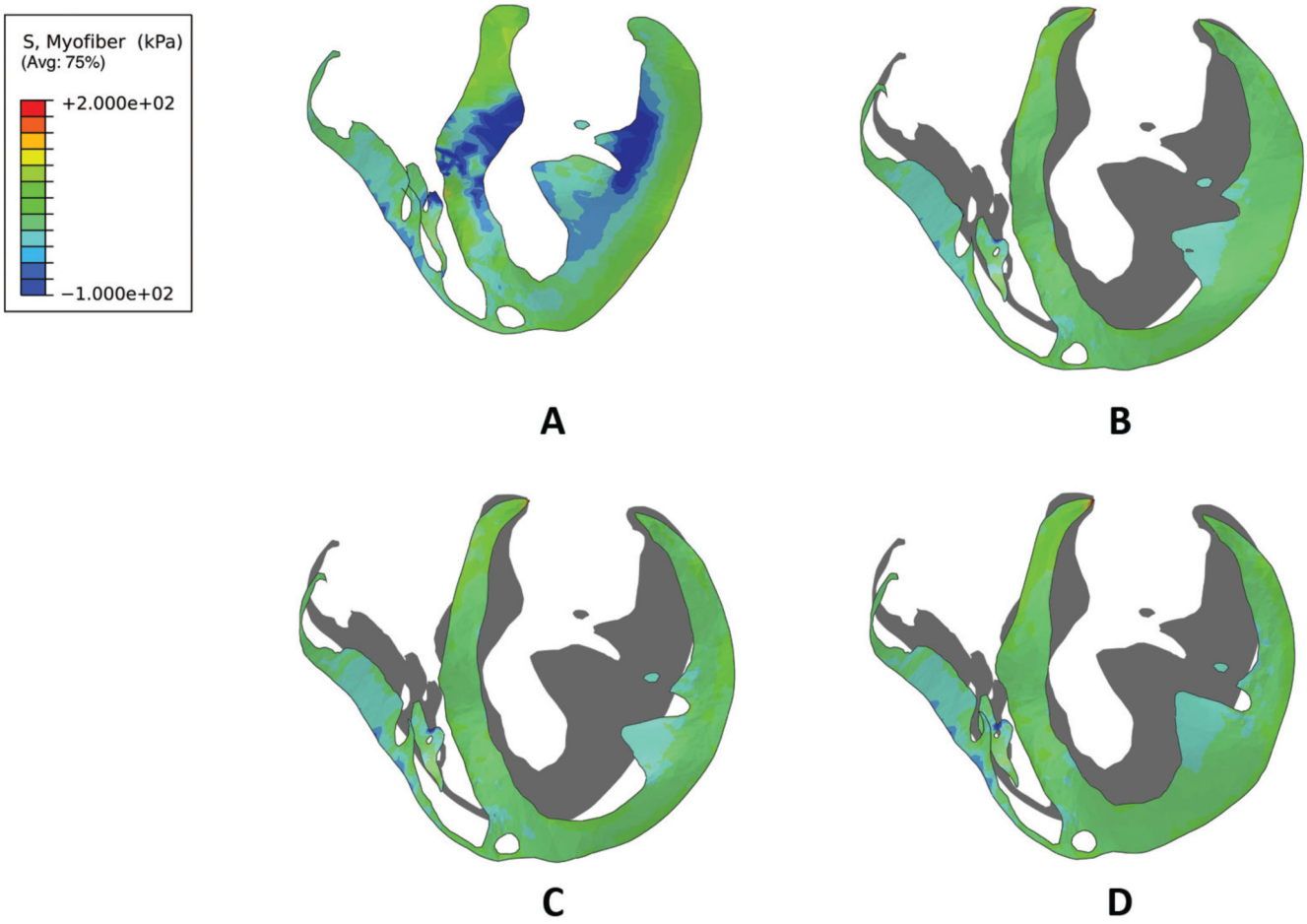

Fig. 5.

Long-axis profiles of the heart at the end of systole showing contours of myofiber stress for a normal healthy heart (**A**), a heart experiencing ALHF (**B**), a heart with ALHF and partial LVAD running at 2 L/min (**C**), and a heart with ALHF and partial LVAD running at 4.5 L/min (**D**). The deformed profile of the normal healthy heart (**A**) is placed behind profiles of cases (**B**) to (**D**) as a grey silhouette for comparison.

Author Manuscript Author Manuscript Author Manuscript Author Manuscript

TABLE I

Constitutive parameters for the passive and active material response

Passive Parameters	**Description**
a,b	Governs the isotropic response of the tissue
a_f,b_f	Governs additional stiffness in the fiber direction
a_s,b_s	Governs additional stiffness in the sheet direction
a_{fs},b_{fs}	Governs coupling stiffness in the fiber and sheet directions
I_1	The first deviatoric strain invariant
I_{4i}	A pseudo-invariant defined as $A_i \cdot C \cdot A_i$
I_{8fs}	A pseudo-invariant defined as $A_f \cdot C \cdot A_s$
C	The Right Cauchy-Green tensor
A_i	Vector in direction i
D	Multiple of Bulk modulus $(K = 2/D)$
J	The third deformation gradient invariant
Active Parameters	**Description**
T_{max}	Constitutive law contractility scaling factor (value directly scales ejection fraction)
Ca_0	The peak intercellular calcium concentration
Ca_{0max}	The maximum intercellular calcium concentration
B	Governs the shape of the peak isometric tension-sarcomere length relation
l_0	The sarcomere length below which no active force develops
t_0	Time to reach peak tension
m,b	Coefficients that govern the shape of the linear relaxation duration and sarcomere length relaxation
E_{ff}	Lagrangian Strain tensor component aligned with the local muscle fiber direction
l_r	The initial sarcomere length

Author Manuscript Author Manuscript Author Manuscript Author Manuscript

TABLE II

Metrics of performance over a cardiac cycle in the normal, acutely failing, and assisted heart

		Normal	ALHF	LVAD 2 L/min	LVAD 4.5 L/min	ALHF	LVAD 2 L/min	LVAD 4.5 L/min
Cavity	**Metric**	**Values**				**% of normal**		
Left Ventricle	EDV (mL)	152.9	206.3	189.8	155.0	135%	124%	101%
	EDP (mmHg)	10.7	27.7	17.6	6.9	259%	164%	64%
	SV = EDV-ESV (mL)	85.5	57.3	37.5	24.0	67%	44%	28%
	Total output (mL)	85.5	57.3	64.4	84.6	67%	75%	99%
	EF (incl. LVAD)	56%	28%	34%	55%	50%	61%	98%
	maxP (mmHg)	135.1	84.3	85.4	97.4	62%	63%	72%
	minP (mmHg)	7.2	19.7	12.5	4.9	274%	174%	68%
Right Ventricle	EDV (mL)	179.9	172.4	175.4	183.0	96%	97%	102%
	EDP (mmHg)	3.3	2.7	2.8	3.1	80%	86%	93%
	SV = EDV-ESV (mL)	84.6	54.7	66.1	84.8	65%	78%	100%
	EF	47%	32%	38%	46%	67%	80%	98%
	maxP (mmHg)	28.6	35.1	30.8	26.6	123%	108%	93%
	minP (mmHg)	0.4	1.9	2.0	2.2	416%	452%	499%

ALHF = acute left heart failure; LVAD = left ventricular assist device; EDV = end-diastolic volume; ESV = end-systolic volume; EDP = end-diastolic pressure; SV = stroke volume; EF = ejection fraction; maxP = maximum ventricular pressure; minP = minimal ventricular pressure.

Author Manuscript

Author Manuscript

Author Manuscript

Author Manuscript

TABLE III

ED and ES volumetric-averaged mean stress results for the normal, acutely failing, and assisted heart presented separately for the LV and RV

Simulation		Normal	ALHF	LVAD 2 L/min	LVAD 4.5 L/min	ALHF	LVAD 2 L/min	LVAD 4.5 L/min
Cavity	**Metric**	**Values (kPa)**				**% of normal**		
LV	ED	1.47 ± 20.72	7.47 ± 35.7	4 ± 29.12	1.26 ± 19.59	508%	272%	85%
	ES	14.45 ± 106.72	16.39 ± 56.81	16.6 ± 56.92	15.81 ± 54.23	113%	115%	109%
RV	ED	1.7 ± 18.06	1.59 ± 16.38	1.6 ± 16.73	1.62 ± 17.47	94%	94%	95%
	ES	1.51 ± 81.78	8.63 ± 74.01	6.89 ± 74.19	5.18 ± 71.52	570%	455%	342%

Results are presented with standard deviations.

ALHF = acute left heart failure; LVAD = left ventricular assist device; ED = end-diastole; ES = end-systole.